ORIGINAL ARTICLE

Vortex-induced vibration (VIV) dynamics of a tensioned flexible cylinder subjected to uniform cross-flow

Bijan Sanaati · Naomi Kato

Abstract This paper presents the experimental results of a study on the effects of axial applied tension on the vibration amplitude, the suppression of vibration, hydrodynamic force coefficients and in-line (IL) and cross-flow (CF) frequency responses during vortex-induced vibration of a horizontally mounted flexible cylinder with a low mass ratio (cylinder's mass/mass of displaced water), low bending-stiffness, and high aspect ratio (length/diameter 200) in the subcritical Reynolds number regime ($Re = 1000$–16000). The effect of tension is studied by applying four different tensions. It was revealed that higher applied tensions, which reduce the vibration amplitude, could significantly raise the hydrodynamic lift force coefficient. In addition, higher applied tensions generate narrower lock-in bandwidths. After the highest vibration amplitude and during the region of lower vibration amplitudes, within the first lock-in region (in the first mode of vibration), power spectral densities show broad bandwidth, while within other regions and higher modes they appear narrow-banded. The ratio of the dominant IL to CF frequency is approximately equal to 2.0, except for the lower reduced velocities, where the ratio values reach 3.83 for the highest tension accompanied by widening of the region in which this ratio is over 2.0. This ratio is 2.76 for the lowest applied tension with a narrower region.

B. Sanaati (✉)
Department of Civil Engineering, Islamic Azad University,
Bookan Branch, West Azarbaijan, Iran
e-mail: sanaaty1@yahoo.com

N. Kato
Department of Naval Architecture and Ocean Engineering,
Graduate School of Engineering, Osaka University,
Suita, Osaka, Japan

1 Introduction

The vortex-induced vibration (VIV) of risers, tensioned leg platform tendons, and sub-sea pipelines subjected to ocean currents, has been a serious concern for ocean researchers and engineers because it imposes high additional costs to projects and has the risk of environmental catastrophe if it is not properly mitigated. Meanwhile, the production of oil, gas, and minerals has extended to deeper oceans in which the risers show very high coupled torsional, axial and lateral flexibility that lead to the inclusion of higher harmonics (excited modal frequencies) in dynamic and vibrational responses at frequencies higher than those resulting from ocean waves and top-end motions of platforms in a very short period. Therefore, these higher modal responses may lead to earlier stress-caused fatigue damage to the riser.

In most real applications, to prevent large deflections in the in-line (IL) direction of a riser's motion due to drag force and to compensate for a riser's weight, an axial force (top tension) is usually applied to the top-end of the riser (Fig. 1). The applied tension may significantly affect the order of IL and cross-flow (CF) excited harmonics, collision avoidance (among adjacent risers) and vibrational suppression. Therefore, the applied tensions seem to play an important role in the dynamic behavior of the riser and may be considered an efficient method for the active control of a riser's statics and dynamics.

Despite many studies dedicated to the problem of elastically mounted rigid cylinders with one or two degrees of freedom [1–5] or flexible cantilevered cylinders [6], few

Fig. 1 Schematic of a real riser configuration
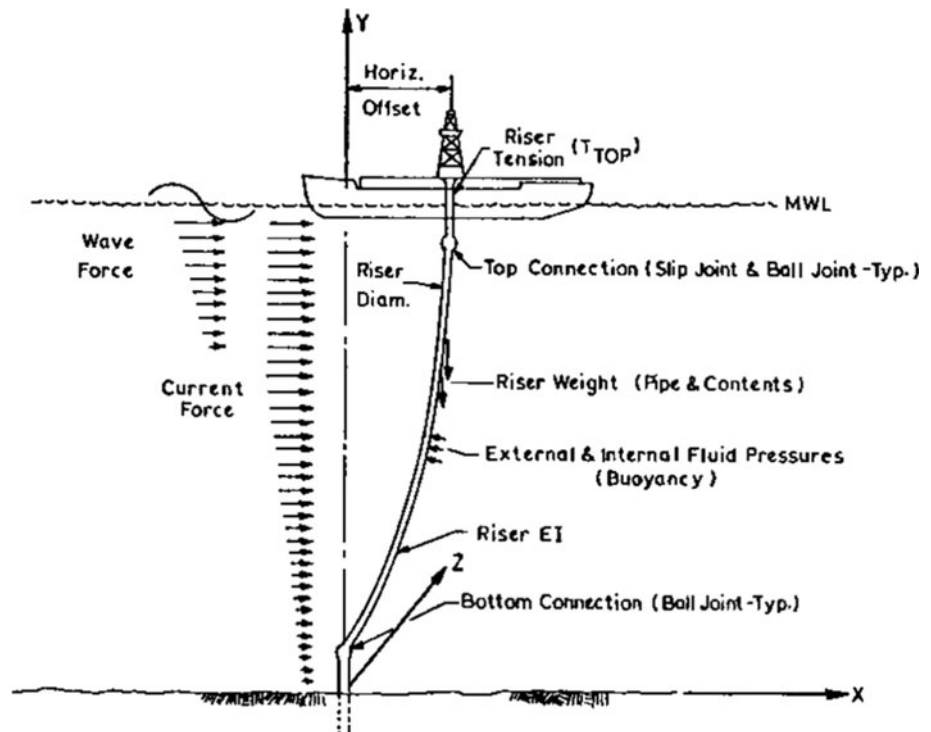
studies have examined the VIV of long high flexible risers with top tension and axial fluctuations. The following shows some features of a few of the preeminent studies published pertaining to top tension application on flexible cylinders.

In a study by Lie and Kaasen [7], a large-scale VIV model with a length of 90 m, a diameter of 3 cm ($L/D = 3000$), a bending stiffness of 364 N m^2, a mass ratio of 3.13 and a top tension of 3700 N subjected to linearly sheared flow was tested. They found that distinct spectral peaks could be observed in only some tests and that there was no evidence of a single mode lock-in.

A comprehensive study performed by Chaplin et al. [8] on a top-tensioned aluminum core riser covered with fluoroplastic pipe with a length of 13.12 m and a diameter of 2.8 cm ($L/D = 468.5$), a high mass ratio of 3.0, a bending stiffness of 29.9 N m^2 subjected to a stepped flow (45 % submerged length) and five applied various tensions (389–1925 N) revealed CF vibrations in up to the 8th mode, with a standard deviation of vibration amplitude ratios of approximately 0.53, which appeared to be widely scattered. They identified the modes of vibration without considering the effects of changes in tension or added mass.

Huera Huarte and Bearman [9, 10] conducted an experiment on a single vertical riser with a length of 1.5 m and a diameter of 1.6 cm (aspect ratio 93.75) subjected to stepped flow (40 % submerged) with a mass ratio of 1.8, a reduced velocity up to 16 and a bending stiffness of

6.04 N m^2. The applied tensions varied from 5.0 to 110 N. They found the maximum CF vibration amplitude ratio (amplitude/diameter) and drag coefficient to be approximately 0.7 and 3.0, respectively, and observed an obvious amplification of the drag with an increasing bi-directional response in the lock-in region with reduced velocities. They only discussed the effect of various applied tensions within the lock-in region of amplitude response for their model (i.e., not lock-in bandwidth, frequency and force responses). They concluded that the vibration amplitude ratio, due to low tensions, is very similar to that of a typical flexibly mounted rigid body with clearly defined initial, upper and lower branches within the lock-in region (defined by Govardhan and Williamson [11]), while for high tensions, the lower branch disappeared. They came to this conclusion despite not having examined a completed lock-in region for higher tensions due to limited flow velocities (the maximum reduced velocity U_r was 6.6 and 7.3, respectively, and the tensions were 85 and 110 N, respectively).

In a study, Lee and Allen [12] examined a vertical ABS riser with a length of 3.72 m and a diameter of 63.5 mm, a pretension of 222.4 N, a bending stiffness of 963.6 N m^2 and a mass ratio of approximately 1.0 and concluded that top tension and structural stiffness (both lateral and axial) can have a significant impact on vibration frequencies and lock-in bandwidth. A further review of this paper will be presented in the test results and discussion section.

Srinil [13] performed numerical simulations to analyze and predict the VIV of variable-tension vertical flexible risers in linearly sheared currents. In his simulations, the effects of tension and sheared flow on the amplitude response and multi-modal VIV are underlined.

To the knowledge of the authors, there is no distinct and detailed discussion or report regarding the effect of top tension on the dynamic responses of a top-tensioned flexible cylinder, especially for hydrodynamic forces and frequency responses. Thus, we set up a system that is capable of applying various tensions to investigate its effects on some of the practical aspects of designing risers and TLP tendons, such as (1) flow-induced vibration and amplitude vibrational suppression, (2) IL and CF frequency response, their harmonics and buildup of higher modes and (3) flow-induced hydrodynamic forces (drag and lift). Compared to previous studies, our test cylinder is tension-dominated with little lateral stiffness, and the whole length is subjected to uniform flow (not sheared flow).

In the first phase of our ongoing research on multiple flexible cylinders, a single flexible cylinder underwent VIV, which has some characteristics (geometrical and mechanical) that are similar to those of real applications. Ocean risers and TLP tendons are tension-dominated (not bending-dominated) in which their ends are pinned and one end is free to slide to limit the lower bound of the tensile stress (Fig. 1). Missing similarities may be listed as sheared CF, high aspect ratio (over 1000) and high Reynolds number in this study. The importance of these three parameters is presented in some of the VIV literature. Spatially sheared flow has been investigated in many studies, such as those by Vandiver et al. [14], Marcollo and Hinwood [15] and Lie and Kaasen [7], and may cause higher harmonics to be included in the VIV response. The response can vary from single mode lock-in to multimodal. Higher aspect ratios confer a very high degree of flexibility to the riser and make the VIV response more complex. Important differences in the dynamic response of flexible bodies arise because of the intrinsic nature of the body, its capacity to vibrate at high mode frequencies and its complex added mass and hydrodynamic damping distribution while in motion [9]. The critical Reynolds number for riser operation in the ocean is above 10^5, according to industry designers. Raghavan and Bernitsas [16] experimentally investigated the effect of the Reynolds number (up to 1.1×10^5) on the VIV of a rigid cylinder on elastic supports. They reported that the range of synchronization of the upper branch increases as the Reynolds number increases, and the maximum amplitude ratio increased to 1.9 for the highest employed Reynolds number. Moreover, the lower branch was overtaken by the extended upper branch.

Our tests revealed some new aspects of this type of VIV with its flexible structure. In the following sections, the experimental set-up, test model characteristics and measurement system are described. Then, the results will be presented and discussed and will be followed by the conclusions and acknowledgments.

2 Experimental set-up

To represent the phenomenon in a more realistic manner, we designed our experiment to have tri-directional oscillations (free to vibrate in IL, CF and axial directions). Ocean risers are always subjected to multi-directional responses. Because the CF oscillation amplitude dominates the amplitude, the IL vibration amplitude is often constrained in laboratory measurements for simplicity. However, as reported by Sarpkaya [17] and Huse et al. [18], the CF amplitude is greater for the free IL case than for the constrained case, and the location of the peak value is different for both cases on the reduced velocity scale.

2.1 Test-model characteristics

A PVC pipe was employed to provide a flexible model with low bending-dependence and an elastic modulus that is approximately one-hundredth that of steel. The cylinder length and diameter are 3600 and 18 mm, respectively. The model was submerged horizontally 0.45 m below the still-water level, which was deep enough to avoid free surface effects. The ends of the model were pinned using universal ball-joints mounted on fixed supports and constrained torsion. One end has no translational movement, and the other is only free for axial-translation (axial sliding). A spring is incorporated at the sliding end to allow the partial axial translation due to the deflected shape induced by the drag force and to ensure that the pipe tensile stress is never exceeded. An axial force is applied to the spring's end. A free-diagram of the deployed system is shown in Fig. 2.

The mass ratio of the horizontal model ($m^* = 4M/\rho\pi D^2$) was assigned to be 1.0 in order to balance the gravity and buoyancy force and thus to keep the cylinder straight without any initial sag. The mass ratio is an important value on the VIV responses. If this parameter is high, the lock-in bandwidth of the amplitude response is very narrow in contrast to a structure with low mass ratio ($m^* < 10$). In addition, the maximum vibration amplitude is lower. More characteristics and parameters of the test cylinder are listed in Table 1.

2.2 Test runs

Experimental tests were performed in the towing tank at Osaka University. The basin is 100 m long, 7.8 m wide and 4.35 m deep. Uniform flows were generated by towing the horizontal cylinder mounted on the carriage at specified
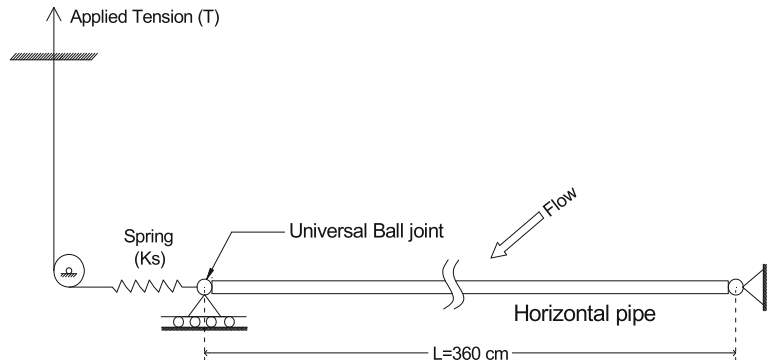
Fig. 2 Free diagram of the test set-up

Table 1 Test cylinder characteristics and parameters

Outside diameter (D)	18 mm
Wall thickness (t)	2.5 mm
Length (L)	3.60 m
Aspect ratio (L/D)	200
Cylinder air weight	1.60 N/m
Total weight-including internal water (M)	2.545 N/m
Applied top-tension (T)	60, 110, 200, 260 N
Mass ratio ($m* = 4M/\rho\pi D^2$)	1.0
(structural plus viscous) Damping ratio (z)	0.025
Bending stiffness (EI/L)	2.7 N m
Spring stiffness (k)	7.6 N/mm
Flow speed (U)	0.05–0.80 m/s
Reynolds number (Re)	1000–16000

speeds. Towing the cylinder horizontally generates non-sheared flow on the cylinder. The flow velocity ranged from 0.05 to 0.8 m/s at increments of 0.05 m/s, which resulted in a range of 1000–16000 for the subcritical Reynolds number.

Measurements were collected over a period of 60 s, but only the data recorded after the carriage accelerated to a constant speed were selected for the analysis. A total of 64 runs were measured for all applied tensions. Each run was started from still water while allowing enough time (10 min) to avoid the initial flow transient effect. Free decay tests were performed by imposing initial displacement at the midpoint of the cylinder to obtain the in-water natural frequency (f_{nw}) and total (structural plus viscous) damping ratio (ζ) of the cylinder for all four applied tensions (Table 2). Natural frequency (Table 2) obtained from the free decay test of $T = 60$ N shows close consistency with that analytical result from the general free vibration equation of motion of an elastic beam under applied axial force (T) (Eq. 1) where M and m_a are the mass per length of the cylinder (including internal water) and added mass (with added-mass coefficient assumed to be 1 in still water), respectively. Up to the fourth mode of vibration has been calculated using Eq. 1 (Table 2).

$$f_n = \left(\frac{n^2\pi}{2L^2}\right)\sqrt{\left(\frac{EI}{M+m_a}\right)}\sqrt{1+\left(\frac{TL^2}{n^2\pi^2 EI}\right)} \quad (1)$$
$$n = 1, 2, 3, \ldots.$$

2.3 Measurement system and data processing

Different kinds of data were recorded during the experiments: the cylinder IL and CF vibration videos and the tensile and hydrodynamic bending strains in the IL and CF directions were done. The tension variations in the towing model were measured using two strain gauges (half-bridge circuit with tension measurement configuration) on opposite sides of the aluminum rod that connected the spring and tension-wire (Fig. 3). For each of the hydrodynamic drag and lift force directions, two half-bridge strain-gauge stations were made at a specified in-between distances (d) of 3 cm (i.e., four stations and eight gauges for both directions). The pair of gauges for each station were installed on opposite sides of the square cross-section of the support rod (Fig. 4) at the fixed-end (not the sliding end-support) of the cylinder between the universal ball-joint and the mounting end-frame (right end in Fig. 2). The hydrodynamic force values could then be calculated using the difference between the bending moment strains of two adjacent measurement stations ($M1$ and $M2$) divided by d (Eq. 2) and calibration coefficients. Calibration tests were carried out using a pulley-weight system for strain measurements in order to convert the bending strain from DC volts unit into N m. Tensile and bending strains were sampled at 200 Hz, which is high enough to obtain precise data.

$$F = (M2 - M1)/d \quad (2)$$

Due to inevitable noise, the data must be preprocessed. Low-pass filtering with a frequency cut-off of 100 Hz was first applied on measured analog data before the data were converted to digital data. The final strains were obtained through low-pass-filtering with a frequency cut off of 60.0 Hz to remove the high frequency (60 Hz) caused by AC current effects of the measurement system.

Table 2 Measured and analytical natural frequencies for various employed pretensions

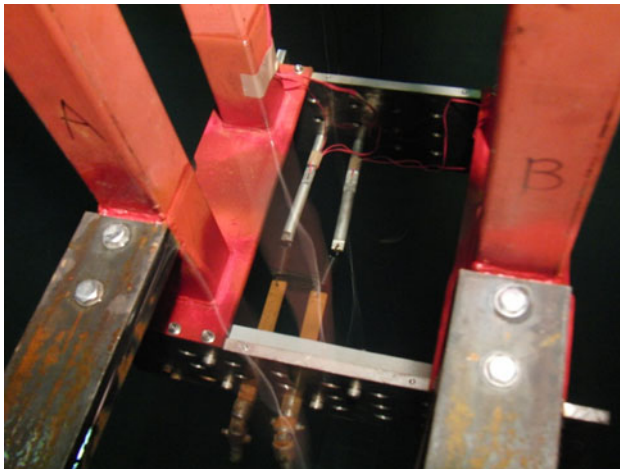| Initial applied tension (N)	Measured natural frequency in water (f_{nw}) 1st mode (Hz)	Analytical natural frequency in air (f_{na}) 1st mode (Hz)	Analytical natural frequency in water (f_{nw})			
			1st mode (Hz)	2nd mode (Hz)	3rd mode (Hz)	4th mode (Hz)
60	1.54	2.26	1.59	3.68	6.57	10.40
110	1.77	2.98	2.10	4.60	7.76	11.76
200	2.34	3.96	2.80	5.90	9.54	13.89
260	2.53	4.50	3.17	6.63	10.55	15.14

Fig. 3 The sliding end of the test set-up where the spring is attached and the initial tension is applied. Universal ball-joints, springs, aluminum rod outfitted with strain-gauges, and other components are shown in this photo
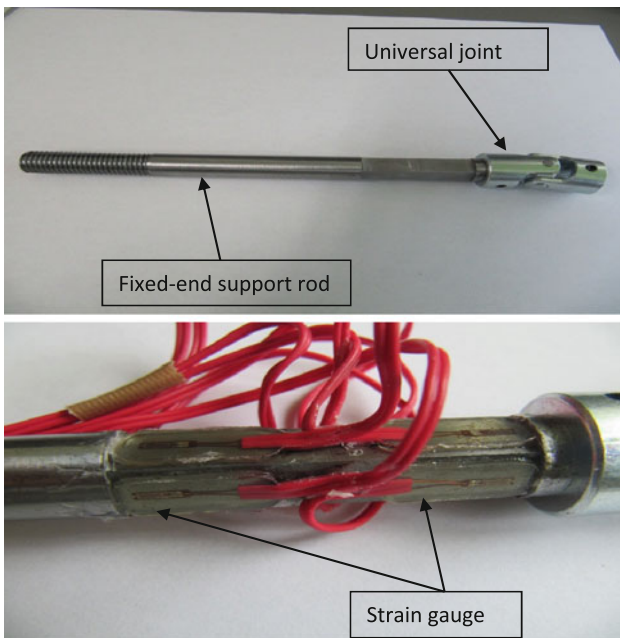

Fig. 4 Eight strain gauges installed on the fixed-end support rod at two stations for the measurement of bending strains in the inline and cross-flow directions

The strain gauges and accelerometers installed inside the cylinder limit and change the cylinder vibrational behavior and their orientation. Therefore, to prevent these problems and avoid the data modification process, underwater CCD cameras were installed above and downstream of the cylinder's middle position at a sufficient distance from the cylinder to visualize the IL and CF vibrations simultaneously (Fig. 5). To avoid wake interference between the cameras and cylinder, the cameras were positioned with a gap of approximately 20D (diameters) above and downstream from the cylinder.

The camera sampling rate was 30 Hz, which resulted in a Nyquist frequency of 15 Hz, which is high enough for CF vibration measurements. Five fluorescent tapes were pasted on the cylinder at 100-mm center-to-center intervals as vibration targets at different positions (Fig. 6). The CF vibration response of only the central target (cylinder's mid-span) is presented and discussed. The cylinder's mid-span target is an anti-node for odd mode-shape numbers and a node for even mode-shape numbers. As described in the following sections, the vibration amplitude is very small for this point during the dominance of the second CF mode shape. We observed the second mode shape from vibration videos when left-hand and right-hand (relative to central tape) tapes had a 180°-phase difference in the vibration and much larger amplitudes than the central tape. The dominance of the second mode of CF vibration response can also be observed from the CF frequency response, which is discussed in the frequency response section.

The camera recordings were also calibrated in three dimensions within the limits of maximum motions. Calibration images along with recorded videos of both IL and CF motions were analyzed simultaneously using the motion tracking commercial software PcMAG (OKK Inc., Japan).

3 Test results and discussion

3.1 Cross-flow vibration results

The dynamic response of the cylinder's vibration is presented in terms of the non-dimensional amplitude ratio,

Fig. 5 A schematic of the cross-section of the experimental set-up, including cameras to record the cylinder vibration
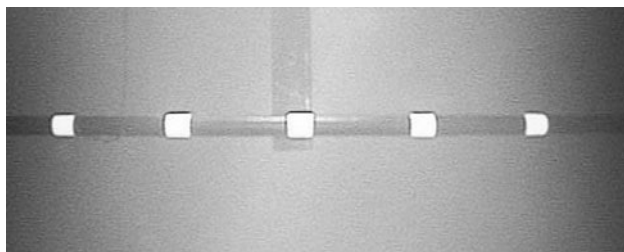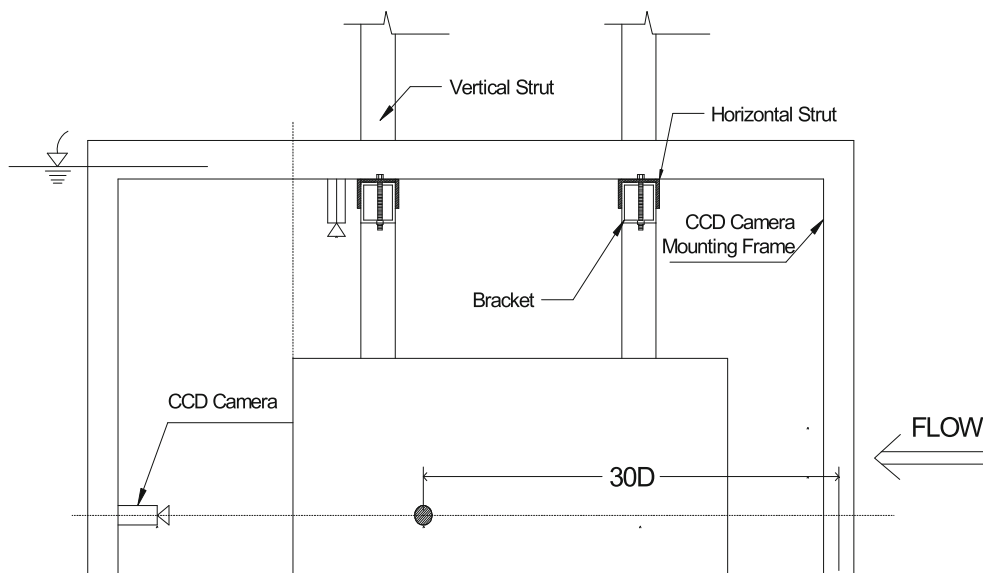

Fig. 6 Five fluorescent tapes as vibration targets were pasted on the cylinder at intervals of 100 mm for center-to-center distances

$A^* = A_{std}/D$, versus reduced velocity, $U_r = U/f_{nw}D$. The value of the vibration amplitude level (A_{std}) is represented in terms of its standard deviation (STD) value calculated by taking the STD of the vibration time series.

3.1.1 Cross-flow vibration amplitude

Amplitude ratios versus reduced velocity (U_r) for all applied tensions (60, 110, 200 and 260 N) are shown in Fig. 7. It is quite clear in this figure that while the tension increases from 60 to 260 N, the maximum vibration amplitude (A^*) decreases by approximately 10 %. The maximum amplitude ratio in the first lock-in region which corresponds to the first peak is 0.64 and 0.57 for tensions 60 and 260 N, respectively.

A comparison between the amplitude responses for the minimum and maximum applied tensions (60 and 260 N) reveals that the lock-in region shifts toward higher flow velocities as the tension increases. This result implies that synchronization will occur at higher flow velocities as its initial tension increases for the same cylinder.
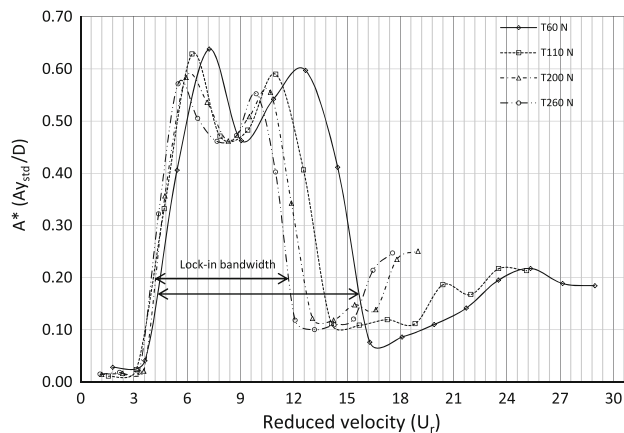

Fig. 7 CF vibration amplitude ratio (A^*) for tensions 60, 110, 200, 260 N versus reduced velocity (U_r)

Govardhan and Williamson [11] reported that two transitions occur in the lock-in region for flexibly mounted rigid cylinders with a low mass-damping ratio ($m^*\zeta$). The first transition involves a 180°-jump in the vortex phase when the vibration frequency becomes equal to in-water natural frequency (transition from initial branch to upper branch of amplitude); while for the second transition, there is a jump in total phase when the vibration frequency becomes equal to the in-air natural frequency (transition from upper branch to lower branch of amplitude). After the second transition, the vortex formation mode faces no change but the total phase difference between CF vibration and lift force becomes 180°.

We cannot characterize the amplitude response based on the phase difference between the time series of vibration and lift force because the force and the vibration are measured at two different locations and the correct phasing

cannot be guaranteed. Hence, we base our discussions on the lock-in phenomenon of the frequencies.

In the present work, the vibration amplitude ratio has a two-hump (peak) shape. The first peak is in the region of synchronization between the first in-water natural frequency (f_{nw}) and the vibration frequency (f_y) of the cylinder. This result corresponds with $U_r = 7.24$ and 5.49 for tensions 60 and 260 N, respectively. After the first peak, there is a decrease down to the trough point, after which the amplitude begins to rise again to another maximum with lower amplitude than the first peak. We should note that any dropping or jumping within response curves can be a sign of transition in the response. Around the trough, the ratio of the vibration frequency to the in-air natural frequency (f_y/f_{na}) should be almost one to ensure that the trough point is the approximate second transition. For instance, the trough point, within the lock-in region of the T60N case, corresponds to the synchronization of the vibration frequency with the in-air natural frequency (f_{na}) of the model since the f_y/f_{na} equals almost one. More explanations about the CF frequency responses and its lock-in characteristics based on obtained frequencies are discussed in Sect. 3.2.1.

The transition can also be inferred from the frequency responses because of the simultaneous sudden increase in the CF and IL frequencies.

It should be mentioned that the second peak due to CF synchronization can also be seen in the drag force

coefficient results, especially for higher initial tensions. Vandiver and Jong [19] found that the drag coefficient is directly related to the energy of the IL and CF responses. They concluded that drag increases with the response going into the larger extent of lock-in. In this situation, the lock-in occurs on a longer length of the cylinder, i.e., spanwise correlation increases.

To achieve a conclusive interpretation of these phenomena, flow visualizations should be performed to determine the transition limits and wake patterns.

Figures 8 and 9 show the time series of CF vibration along with the corresponding power spectral density (PSD) within the first lock-in region for T60N and T260N, respectively. From Fig. 7, the lock-in region occurs at $0.15 < U < 0.35$ and $0.20 < U < 0.45$ m/s for tensions of 60 and 260 N, respectively. The maximum vibration amplitude of the cases T60N and T260N occurs at around the $U = 0.20$ m/s and $U = 0.25$ m/s, respectively. The measured natural frequencies of the cylinder at T60N and T260N cases are 1.54 and 2.53 Hz, respectively (Table 2). From the PSDs of force signals and those of CF vibration at the T60N and T260N cases, we observe that the dominant frequencies in the PSDs of lift force and CF vibration are close in value to the mentioned natural frequencies at the $U = 0.20$ m/s and $U = 0.25$ m/s, respectively, which indicates that the response is in resonant mode.
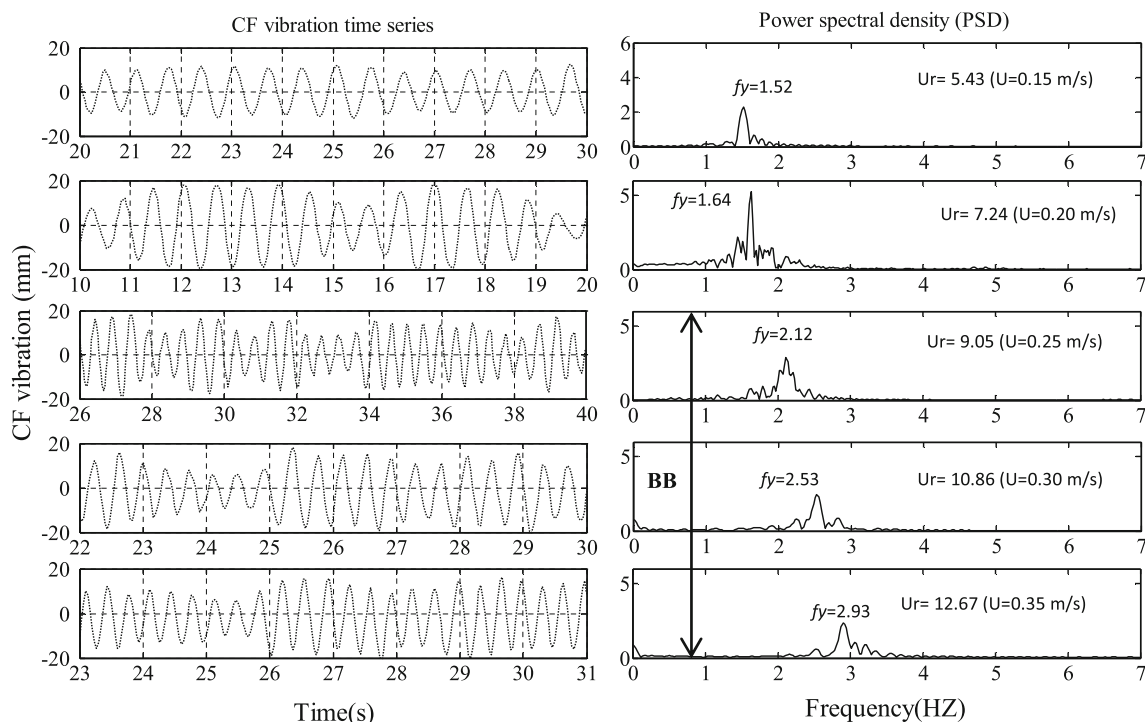

Fig. 8 The time series of the CF vibration along with their corresponding spectral response in the expected lock-in region ($0.15 < U < 0.35$ m/s) for the case of tension 60 N. "BB" denotes broad-banded regions of the frequency responses
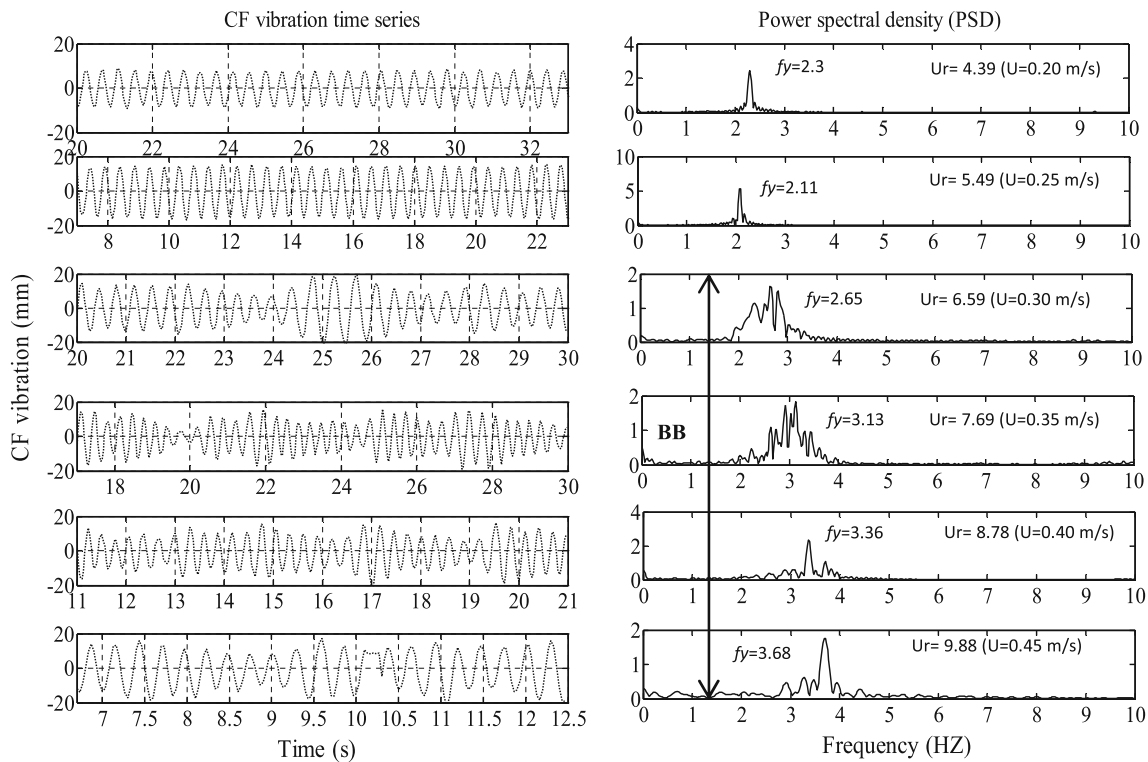
Fig. 9 The time series of the CF vibration along with their corresponding spectral response in the expected lock-in region ($0.20 < U < 0.45$ m/s) for the case of tension 260 N. "BB" denotes broad-banded regions of frequency responses

3.1.2 Lock-in bandwidth

The lock-in bandwidth is essential to study because it is used by designers to determine potentially harmful reduced velocities. A broad-band signal indicates a wide range of critical non-dimensional velocities. A comparison among vibration amplitude ratios (A^*) and first lock-in bandwidths for all four applied tensions has been presented (Fig. 7). We can easily observe that the amplitude graphs corresponding to tensions 60 and 110 N have an apparent broader lock-in bandwidth than tensions 200 and 260 N. This result indicates the considerable effects of applied tension on the flexible cylinder vibration response. In fact, CF lock-in bandwidth decreases as the pretension value increases because the tension causes the natural frequencies to increase and the reduced velocity to decrease. In addition, for a heavier and stiffer structure, the response will be small, which reduces the width of the lock-in range [12]. Because our test cylinder is not heavy (mass ratio is low), it is only higher tension, compared to lower tensions, which adds to the total stiffness of the structure and results in a narrower lock-in bandwidth.

3.2 Frequency responses results

Frequency responses are obtained through frequency analysis of force signals using the fast Fourier transform

function (FFT) rather than cylinder oscillation data because the force data sampled at a frequency of 200 Hz (30 Hz for oscillation data) gives more reliable frequency values in both IL and CF directions. Dominant IL and CF frequencies (the frequency with the maximum amplitude) have been summarized and shown in Fig. 10 in the form of their ratio to the first natural frequency, i.e., f_x/f_{nw}, and f_y/f_{nw}. It is noted that the frequency ratios (f_x/f_{nw} and f_y/f_{nw}) based on the first in-water natural frequency (f_y/f_{nw}) cannot be a good criteria for finding the mode numbers, especially for low applied tension values because as mentioned in Sect. 3.1.2, the natural frequency increases with reduced velocity for low mass cylinders.

3.2.1 Cross-flow frequency response

Bending-dominated risers have a slight increase in vibration frequency after an abrupt rise to their first lock-in frequency because the motion of the structure takes control of the shedding process. However, for tension-dominated risers, there is a significant rise to the vibration frequency after each lock-in [12]. This phenomenon can be seen clearly from Fig. 10 (CF vibration frequency ratio (f_y/f_{nw}) vs. reduced velocity). In other words, the vibration frequency increases monotonically during each lock-in occurrence and before lockout.
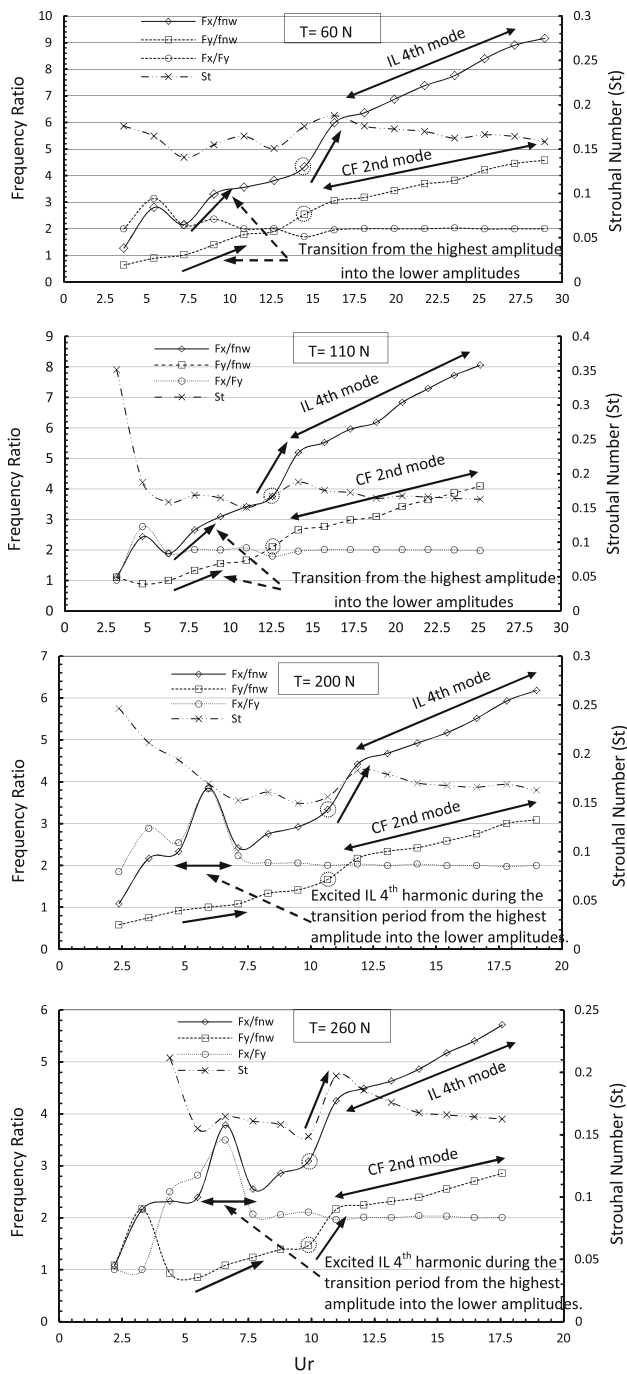
Fig. 10 IL, CF and IL-to-CF frequency ratios for tensions 60, 110, 200, 260 N versus reduced velocity (U_r). Strouhal number is also shown. *Single arrows* show the different transitions between response regions. *Horizontal double arrows* show the region in which the IL 4th harmonic is excited during the transition period from the highest amplitude into the lower amplitudes for higher tensions
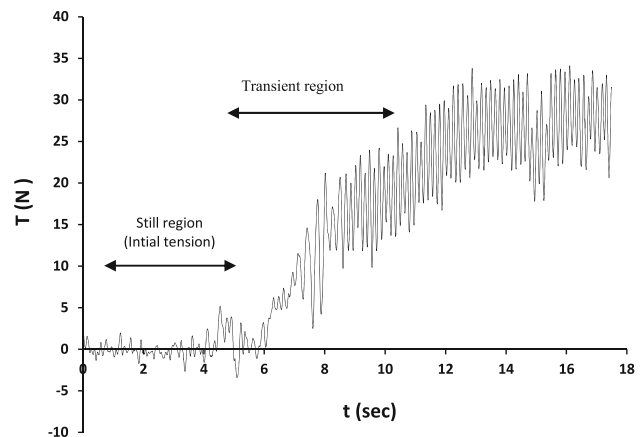

Fig. 11 Time series of the increased applied tension for an initial tension of 260 N and a flow velocity of 0.7 m/s. The initial value of tension has been subtracted from the values shown

tension. Note that, for a bending-dominant riser, the IL force is resisted by the bending stiffness, and the tension increase is small. However, other studies related this phenomenon (rise of the vibration frequency during a lock-in occurrence) to cylinders with low mass ratios with $m^* < 10$ (e.g., Khalak and Williamson [20]).

The measured tension of our experiment showed increases and fluctuations (Fig. 11). The results shown for the tension is its increase from the initial value. We subtracted the initial tension value from the measured tension. Because we do not have experimental results for a bending-dominated cylinder, we cannot relate this phenomenon strictly to the tension increase, although it is a plausible explanation. Our future experiment will focus on this matter.

In Fig. 10, the CF frequency response ratio versus the reduced velocity is shown for all applied initial tensions. The horizontal grid-line with the value of 1.0 corresponds to the first synchronization between the in-water natural frequency (f_{nw}) and the CF frequency. Along with the frequency ratios, Fig. 10 also includes the Strouhal numbers (St) for all the data points and test cases. The Strouhal number, like the frequency ratios, shows a sudden jump at the point of vibration transition to higher modes. However, its value gradually decreases just before the transition. For our experiments, Strouhal numbers range from 0.155 to 0.17, except for the region of lower reduced velocities Dashed open circles show the points just before the mode number switches to the subsequent mode. This switch occurs in the form of a sudden jump of the solid line, as also reported by Chaplin et al. [21]. These switches usually occur in a very small range of reduced velocities. In addition, there is a region where the frequency responses experienced a sudden change or increase shown by a double arrow and/or a single arrow for IL and CF directions. The trough point in Fig. 7 is located in this region. In

Lee and Allen [12] concluded that it is the change in tension due to the increased drag force with current that is primarily responsible for the rise of the vibration frequency in the lock-in region and the key to the vibration frequency is the rise of tension, regardless of the magnitude of applied

this region, the CF frequency response has jumped to upper values (shown by single arrows), close to natural frequency in air, which corresponds to the transition in the response. The IL frequency response also jumped to higher values at T60N and T110N cases (shown by single arrows) and switched temporarily to its fourth mode at T200N and T260N cases during the transition period (refer to Sect. 3.2.2 for details).

The maximum frequency ratios (f_y/f_{nw}) corresponding to the maximum flow velocity of 0.8 m/s tested for tensions of 60 and 260 N are 4.60 and 2.87, respectively, which implies that higher applied tension, compared to lower tension, can postpone the excitation of higher modal frequencies within the same range of flow velocities.

3.2.2 In-line frequency response

The IL response frequency usually occurs twice at the CF response and the mode number. However, this phenomenon does not occur for low reduced velocities in which IL lock-in happens. King et al. [22] reported the ratios of IL vibration frequency to dominant wake frequency as 4, 3.5, 3, 2.15 and 2 throughout the IL lock-in range ($1.5 < U_r < 3.5$) for a flexible cantilever. Huse et al. [18] reported that the IL excitation frequency was four times greater than the CF excitation at low reduced velocities. Moreover, on an elastically mounted rigid cylinder, Fujarra and Pesce [23] found that the IL frequency response jumps to four times the natural frequency at values of $U_r > 5.0$. A recent study on the flexible vertical cylinder exposed to shear flow by Marcollo and Hinwood [15] concluded that the dominant IL excitation frequency at four times the predicted shedding frequency provides a power-in effect to support the dominant mode's CF response.

Figure 10, in addition to the CF frequency response, also includes a non-dimensional IL frequency response along with the ratio of IL to CF dominant frequency responses for all applied initial tensions. Our objective when presenting these results is not only to verify their findings but also to investigate the effect of various tensions on the frequency response, particularly the ratio of IL to CF frequency responses. The features of frequency analysis, shown in Fig. 10, are summarized as follows.

(a) As discussed in the section describing the CF amplitude frequency response, jumps in frequency for both the IL and CF directions occur denoting the build-up of new upper vibration mode-shapes. It is interesting to note that both frequency responses begin to jump to higher modal frequency responses at the same reduced velocities (shown by open circles) and the jumps occur immediately after the lock-out of the first lock-in region.

(b) The IL frequency and CF frequency at reduced velocities of 3.14 for T110N and 1.10 and 2.20 for T260N are equal. This result may, as also reported by Chen and

Jendrzejczyk [24], correspond to the IL first instability lock-in region. For T260N at a reduced velocity of 2.20, the cylinder vibrates at its second modal frequency in both the IL and CF directions.

(c) For all tensions, the ratio of IL frequency to CF frequency almost equals 2.0, except for lower reduced velocities, i.e., $U_r < 7.24$, 6.27, 7.13 and 5.49 for T60, 110, 200 and 260 N, respectively. The maximum IL-to-CF ratio for lower reduced velocities reaches 3.14, 2.76, 3.83 and 3.50 for T60, 110, 200 and 260 N, respectively. It is evident that this ratio increases for higher tensions accompanied by widening of the region in which this ratio is over 2.0. In other words, there is more than one flow velocity for higher tensions (T200, 260 N) in which the ratio exceeds 2.0 ($f_x/f_y > 2$) exist.

3.2.3 Spectral description of force time series

Measured force time series and their corresponding PSDs for tensions 60 and 260 N over all tested velocities (0.1–0.8 m/s) have been shown in Figs. 12 and 13. We can easily observe from these figures that more than one modal frequency have been excited (multi-modal response) in the CF response for low reduced velocities and in the IL response direction for most of the velocities tested. Moreover, the CF frequency can be recognized from the PSDs of IL response. Modulation (beating) can also be recognized for IL and CF force time series. The dominant frequencies (the frequency with the maximum amplitude) have been summarized and are shown in Fig. 10. For the flow velocities at which the vibration amplitude regime has switched to the region with lower amplitude within lock-in region, PSDs show the broad bandwidth comprising many frequencies, while for the other regions and higher modes, the PSDs are narrow-banded. Broad-banded PSDs are determined in Figs. 12 and 13 with BB (broad-banded) symbols. This symbol is also shown in Figs. 8 and 9.

3.3 Hydrodynamic force coefficients

In general, IL and lift force coefficients are found to be larger than those measured for short sections of cylinders undergoing free and forced (one or two-dimensional) motions [25]. This section presents the analysis results of the measured hydrodynamic forces (refer to Sect. 2.3 for force measurement system), namely, the drag and lift in the form of their corresponding coefficients for various tensions. The mean drag (CD_{mean}), fluctuating drag (CD_{rms}) and fluctuating lift (CL_{rms}) coefficients were computed by taking the mean and root-mean-square (rms) values of the time series of measured force, respectively, at the end of the cylinder exposed to the uniform CF over its whole length (Eqs. 3 and 4). Parameter ρ is water density, while F_D and F_L are the corresponding decomposed mean and
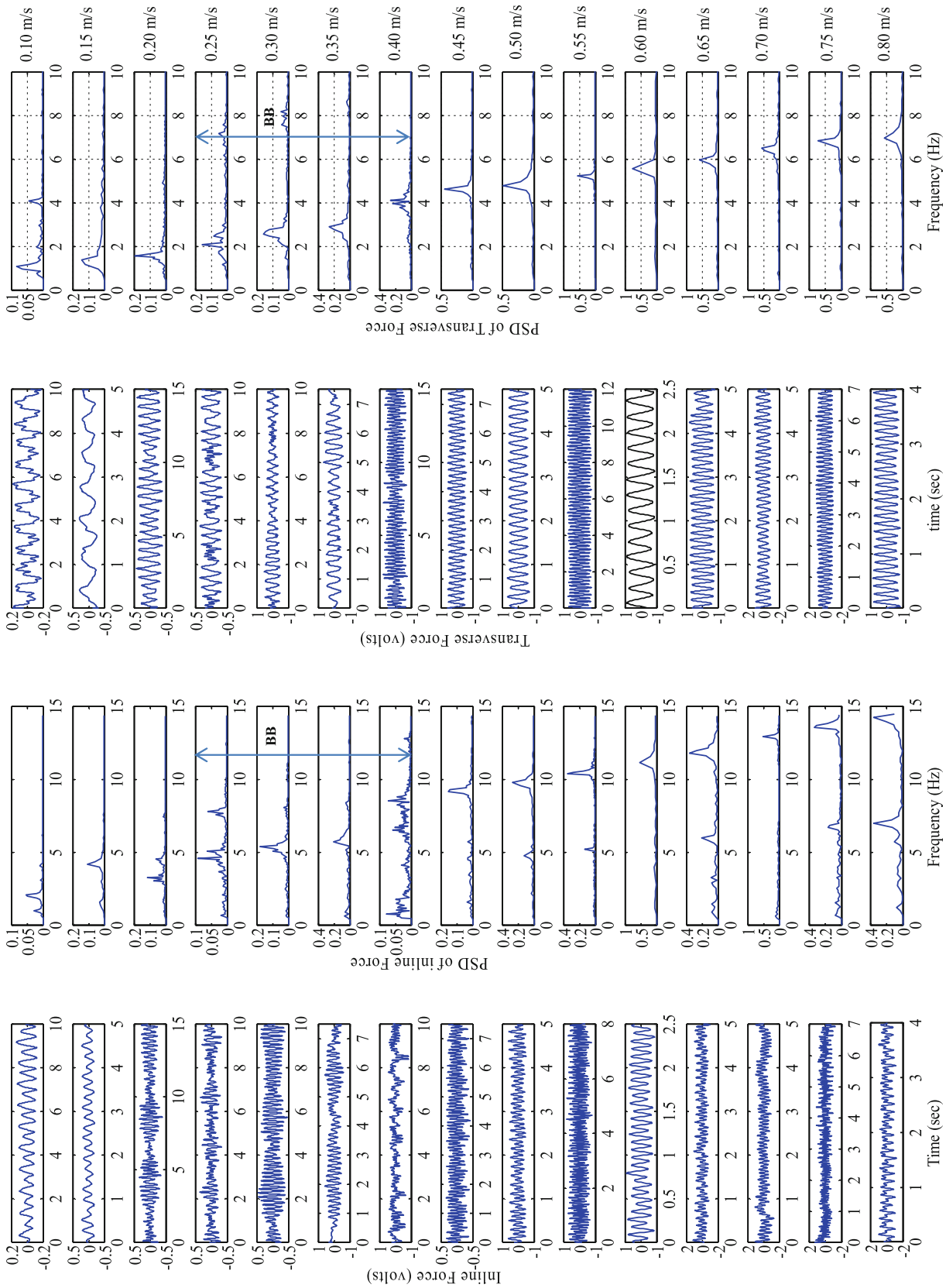
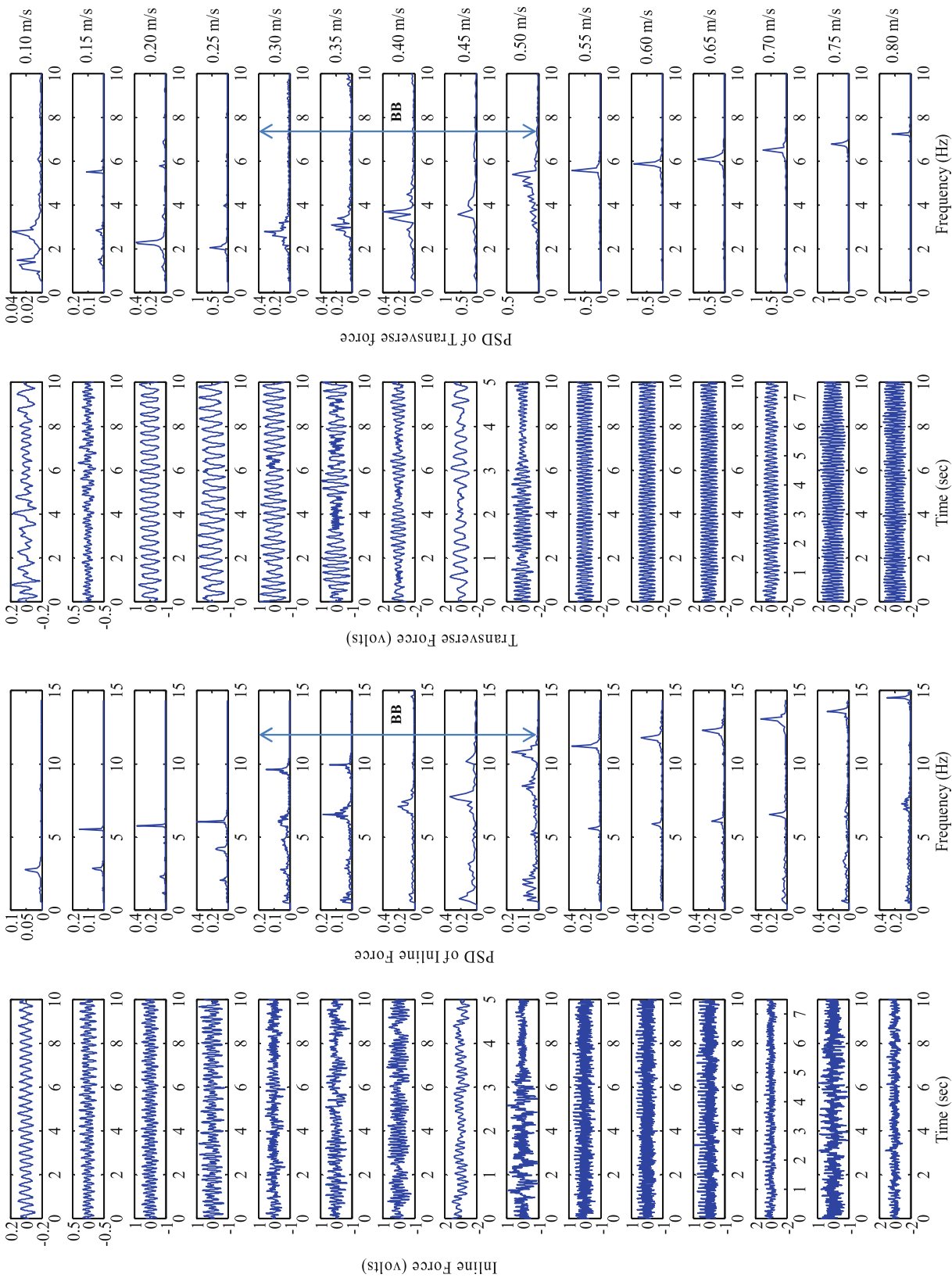**Fig. 12** Drag and lift force time series along with their respective PSDs for tension of 60 N

Fig. 13 Drag and lift force time series along with their respective PSDs for tension of 260 N
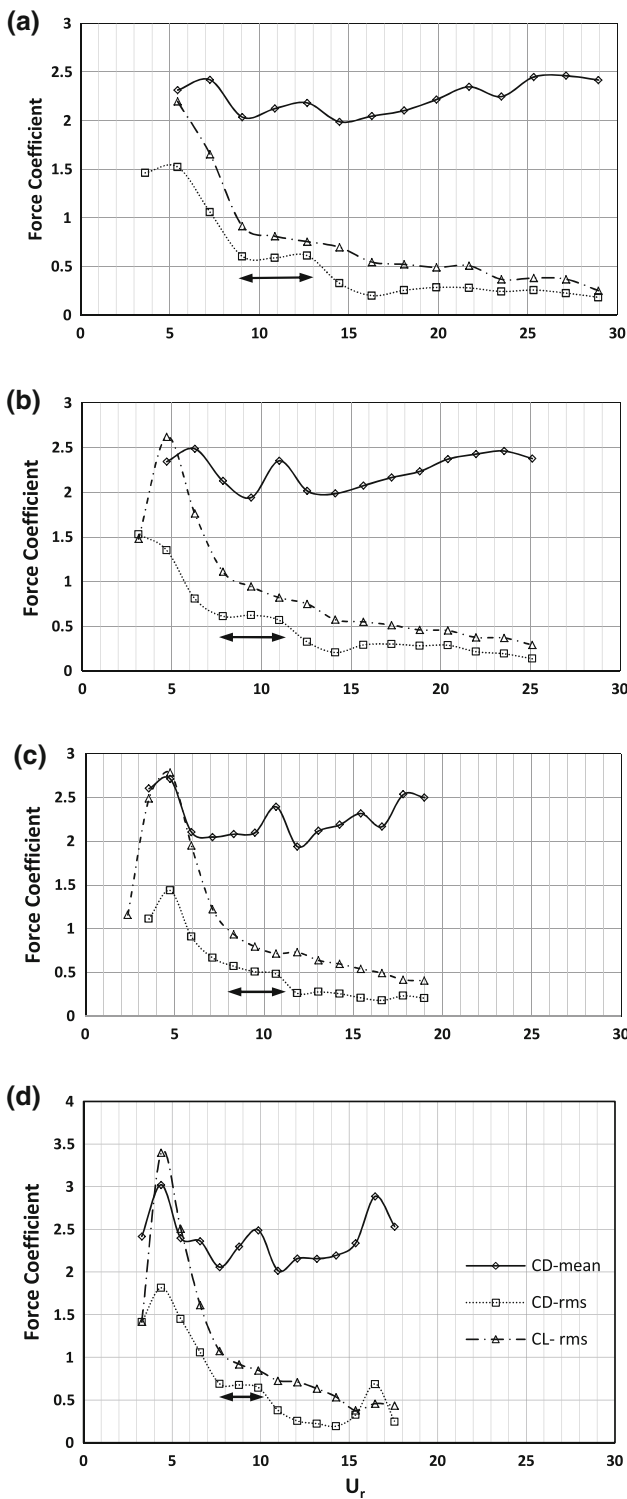
Fig. 14 Hydrodynamic drag and lift force coefficients for tensions: **a** 60 N, **b** 110 N, **c** 200 N and **d** 260 N versus reduced velocity

fluctuating terms, respectively, of the total forces in the IL and CF directions.

$$C_D = \frac{F_D}{1/2\rho U^2 LD} \qquad (3)$$

$$C_L = \frac{F_L}{1/2\rho U^2 LD} \qquad (4)$$

Figure 14 shows the hydrodynamic force coefficients for each of the applied tensions in graphs (a) through (d), from which many features can be inferred. The features of Fig. 14 are described in the following by comparing the obtained results of all tensions:

(a) The magnitude of all hydrodynamic force coefficients increases as the initial applied tension increases. The maximum value of the mean IL force coefficients (CD_{mean}) for tensions 60, 110, 200 and 260 N are 2.42, 2.49, 2.71, and 3.02, respectively. The lift force coefficients at the respective tensions are 2.20, 2.62, 2.78 and 3.40. These results correspond with an approximately 55 % increase in the lift force coefficient. As already discussed in the section on the vibration amplitude response, the vibration amplitude (in contrast to the considerable increase in forces) decreases slightly as the applied tension increases. The force increases with tension because the higher applied tension increases the cylinder's overall stiffness, which in turn increases the cylinder's resistance to large oscillation and IL deflection, and thus, larger forces will be generated on the cylinder. In other words, if the stiffness of a structure increases, its reaction forces increase and the vibration amplitude or deflection decreases.

(b) The maximum values of force coefficients at all tensions belong to the first lock-in region. The force coefficients have peaks in the regions of the highest vibration amplitude. These peaks coincide with those of the vibration amplitude except for the first peak (in the first lock-in region). The first peaks of the drag and lift forces occur around the point of first transition; while for vibration, the first peak occurs in the maximum amplitude region. This transition normally occurs after the cylinder vibration amplitude reached its half maximum value, i.e., $A^* \approx 0.5\, A^*_{max}$. For amplitude ratios larger than $0.5\, A^*_{max}$, the forces decrease, and the amplitude ratio (A^*) reaches a self-limiting value [2, 17]. In other words, the largest drag and lift force coefficients are related to their respective largest synchronized CF vibration amplitude regions.

(c) Finally, it is worth noting that the continuous dropping of unsteady IL force coefficient (CD_{rms}) occurs after the maximum amplitude, and then the IL force coefficient is approximately constant within the lower amplitude region (double arrows in Fig. 14). The mean IL force increases, including several peaks that correspond to vibration amplitude peaks. Huera Huarte and Bearman [9] concluded that as the amplitude and synchronization of the biharmonic, synchronized response starts to decrease, the drag also decreases, which leads to values similar to those of stationary cylinders at the same Reynolds number (Re). His conclusion is in direct

contrast to what we have found. After the first synchronization peak, the fluctuating lift force coefficient (CL$_{rms}$), unlike the fluctuating IL component, decreases continuously with the reduced velocity. This phenomenon occurs, perhaps because of the continuous decrease in the added-mass coefficient of the inertia component of the lift force with reduced velocity.

4 Conclusions

This paper presents the vibration amplitude and hydrodynamic force (drag and lift) analysis results during the VIV of a horizontally mounted flexible cylinder with a low mass ratio, a subcritical Reynolds number range, a low bending stiffness, and a high aspect ratio with various applied tensions. The top tension affects the vibration amplitude and hydrodynamic forces of risers and is considered an efficient tool for the active control of the statics and dynamics of risers. It was revealed that higher applied tensions, which lead to smaller vibration amplitudes, can significantly increase the hydrodynamic lift force. Decreasing the fluctuating component of drag and lift forces causes different behaviors due to the added-mass effect. Higher applied tension generates narrower lock-in bandwidth. At all tensions, the ratio of dominant IL to CF frequency (f_x/f_y) equals almost 2, except for lower reduced velocities ($U_r < 7.24$ and 5.49 for Tensions 60 and 260 N, respectively), where the ratio values reached 3.83 for higher tensions and were accompanied by widening of the region in which this ratio is over 2. The ratio was 2.76 for lower tensions with narrower regions. During the flow velocities in which the cylinder's vibration has transitioned to the lower amplitudes within lock-in region, PSDs bandwidth comprising many frequencies (broad-banded), while for other regions within lock-in and higher modes regions, they appear narrow-banded.

Further work is needed to investigate the effects of changes in tension due to induced drag force on the VIV response. In addition, to obtain a comprehensive understanding of the effects of various tensions on VIV responses, higher Reynolds numbers and aspect ratios should be taken into account in future works. Employing the particle image velocimetry technique (PIV) can provide a better understanding of wake patterns and transition points.

References

1. Bearman PW (1984) Vortex shedding from oscillating bluff bodies. Annu Rev Fluid Mech 16:195–222
2. Sarpkaya T (2004) A critical review of the intrinsic nature of vortex-induced vibrations. J Fluids Struct 19:389–447
3. Williamson CHK, Govardhan R (2004) Vortex-induced vibrations. Annu Rev Fluid Mech 36:413–455
4. Assi GRS, Bearman PW, Meneghini JR (2007) Unsteady force measurements on a responding circular cylinder in the wake of an upstream cylinder. In: Proceedings of the 26th international conference on offshore and arctic mechanics (OMAE2007), paper no. 29040
5. Brankovic M, Bearman PW (2006) Measurements of transverse forces on circular cylinders undergoing vortex-induced vibration. J Fluids Struct 22:829–836
6. Prastianto RW, Otsuka K, Ikeda Y (2009) Hydrodynamic forces on multiple free-hanging circular cantilevers in uniform flows. Int J Offshore Polar Eng (IJOPE) 19(2):108–114
7. Lie H, Kaasen KE (2006) Modal analysis of measurements from a large-scale VIV model test of a riser in linearly sheared flow. J Fluids Struct 22:557–575
8. Chaplin JR, Bearman PW, Huera Huarte FJ, Pattenden RJ (2005) Laboratory measurements of vortex-induced vibrations of a vertical tension riser in a stepped current. J Fluids Struct 21:3–24
9. Huera Huarte FJ, Bearman PW (2009) Wake structures and vortex-induced vibrations of a long flexible cylinder—part 2: drag coefficients and vortex modes. J Fluids Struct 25:991–1006
10. Huera Huarte FJ, Bearman PW (2009) Wake structures and vortex-induced vibrations of a long flexible cylinder—part 1: dynamic response. J Fluids Struct 25:969–990
11. Govardhan R, Williamson HK (2000) Modes of vortex formation and frequency response of a freely vibrating cylinder. J Fluid Mech 420:85–130
12. Lee L, Allen D (2010) Vibration frequency and lock-in bandwidth of tensioned, flexible cylinders experiencing vortex shedding. J Fluids Struct 26:602–610
13. Srinil N (2011) Analysis and prediction of vortex-induced vibrations of variable-tension vertical risers in linearly sheared currents. J Appl Ocean Res 33:41–53
14. Vandiver JK, Jaiswal V, Jhingran V (2009) Insights on vortex-induced, traveling waves on long risers. J Fluids Struct 25:641–653
15. Marcollo H, Hinwood JB (2006) On shear flow single mode lock-in with both cross-flow and in-line lock-in mechanisms. J Fluids Struct 22:197–211
16. Raghavan K, Bernitsas MM (2011) Experimental investigation of Reynolds number effect on vortex-induced vibration of rigid cylinder on elastic supports. J Ocean Eng 38:719–731
17. Sarpkaya T (1995) Hydrodynamic damping, flow induced oscillations, and biharmonic response. J Offshore Mech Arct Eng 71:232–238
18. Huse E, Nielsen FG, Soreide T (2002) Coupling between in-line and transverse VIV response. In: Proceedings of the 21st international conference on offshore and arctic mechanics (OAME2002), paper no. 28618
19. Vandiver JK, Jong JY (1987) The relationship between in-line and cross-flow vortex-induced vibration of cylinders. J Fluids Struct 1:381–399
20. Khalak A, Williamson CHK (1999) Motions, forces and mode transitions in vortex-induced vibrations at low mass-damping. J Fluids Struct 13:813–851
21. Chaplin JR, Bearman PW, Huera Huarte FJ, Pattenden RJ (2004) Laboratory measurements of vortex-induced vibrations of a

vertical tension riser in a stepped current. In: Proceedings of flow induced vibration conference (FIV2004), pp 279–284

22. King R, Prosser MJ, Johns DJ (1973) On vortex excitation of model piles in water. J Sound Vib 29:169–188

23. Fujarra A, Pesce C (2002) added mass of an elastically mounted cylinder in water subjected to vortex-induced vibrations. In: Proceedings of 21th international conference on offshore mechanics and arctic engineering (OMAE2002), pp 1–6

24. Chen SS, Jendrzejczyk JA (1979) Dynamic response of a circular cylinder subjected to liquid cross-flow. J Press Vessel Technol 101:106–112

25. Bearman PW, Huera Huarte FJ, Chaplin JR (2006) The hydrodynamic forces acting on a long flexible circular cylinder responding to VIV. In: Proceedings of sixth ASME international conference on FSI, AE and FIV, pp 611–619